International Journal of Hydrogen Energy 170 (2025) 150980

Contents lists available at ScienceDirect

International Journal of Hydrogen Energy

journal homepage: www.elsevier.com/locate/he

Effect of natural gas impurities on electrochemical hydrogen compression and strategies for mitigation

Wibke Zängler [a], Nick Semrau [a], Matthias Wessling [a,b], Robert Keller [a,*]

[a] RWTH Aachen University, Chemical Process Engineering, Forckenbeckstr. 51, Aachen, 52074, Germany
[b] DWI - Leibniz Institute for Interactive Materials, Forckenbeckstr. 50, Aachen, 52074, Germany

ARTICLE INFO

Keywords:
Electrochemical hydrogen compression
Poison mitigation
HOR
Polybenzimidazole
Hydrogen withdrawal from natural gas

ABSTRACT

Admixing of H_2 into the natural gas grid is a viable option for mid-term transportation. Electrochemical H_2 compressors (EHCs) separate H_2 from methane but are prone to poisoning due to impurities. This study compares low- and high-temperature EHCs regarding their tolerance towards natural gas impurities, focusing on the underexplored contaminants NH_3 and H_2S and mitigation strategies. The impact of impurities was evaluated using 5 h chronopotentiometry, cyclic voltammetry, and electrochemical impedance spectroscopy. Low-temperature EHC (70 °C) showed an increase of up to 200 % in cell potential, while the increase remained below 6 % for high-temperature EHC (120 °C), when operated with CO_2, CO, or H_2S. When diluting the H_2/H_2S mixture in the high-temperature EHC with CH_4, oscillations and an increase in cell potential were observed, which was mitigated when operating at 160 °C or via electro-oxidation. The results establish a foundation for long-term stability testing in natural gas.

1. Introduction

Until 2030, several EU countries want to leverage H_2 admixing to the natural gas grid for H_2 distribution as an interim step for decarbonization [1,2]. Distributing H_2 by blending it into the existing natural gas grid could reduce the cost of transportation in the mid-term future and facilitate H_2 supply to remote locations [3]. Moreover, it would enable H_2 injection into the natural gas during off-peak hours. At the point of use, separation and compression technology is needed for local withdrawal of H_2. State-of-the-art technologies for H_2 separation are pressure-driven membranes for moderate purity combined with pressure swing adsorption (PSA) for high purities above 98 %. In PSA, multiple adsorption columns packed with adsorbent are employed [4]. PSA units are usually operated on a large scale and are economically less attractive for small-scale H_2 separation [5]. The size of the PSA plant increases with lower H_2 concentrations in the feed gas stream [6]. Moreover, H_2 recovery rates for small-scale PSA are low (<75 %) [4], and additional compression capacity is needed. Electrochemical hydrogen compression is a promising alternative technology, especially for distributed H_2 withdrawal.

Fig. 1 illustrates the working principle of an electrochemical hydrogen compressor (EHC) and the challenges of low- and high-temperature EHC. On the EHC's anode, H_2 from a pure feed or a gas mixture is selectively oxidized (hydrogen oxidation reaction (HOR), Eq. (1)). The formed protons migrate towards the cathode governed by the electrical driving force applied to the system. On the cathode, the protons are reduced, and H_2 at a higher partial pressure evolves (hydrogen evolution reaction (HER), Eq. (2)) [7,8].

$$H_2 \longrightarrow 2\,H^+ + 2\,e^- \tag{1}$$

$$2\,H^+ + 2\,e^- \longrightarrow H_2 \tag{2}$$

The increase in H_2 partial pressure from the anode (p_a) to the cathode side (p_c) is governed by the Nernst potential E_N (Eq. (3)) with R the ideal gas constant, T the process temperature, $n = 2$ the number of electrons transferred in the reaction, F the Faraday constant. For the EHC, the Nernst equation simplifies as the standard potential of the hydrogen oxidation and evolution is 0 V vs. SHE.

$$E_N = \frac{RT}{2F} \ln \frac{p_c}{p_a} \tag{3}$$

An EHC offers high recovery rates and H_2 purity in a single step while maintaining high efficiency, also in small-scale operation [9,10]. Additionally, EHC combines H_2 compression and separation in one unit operation, being a key advantage for application with impure H_2 or gas mixtures such as blended natural gas [11].

The main challenges for implementing the EHC in the natural gas grid are the proper humidification of the mostly perfluorinated sulfonic acid (PFSA)-based proton exchange membranes (PEMs), high

* Correspondence to: RWTH Aachen University, Aachener Verfahrenstechnik - Chemical Process Engineering, Forckenbeckstr. 51, 52074 Aachen, Germany.
E-mail address: robert.keller@avt.rwth-aachen.de (R. Keller).

https://doi.org/10.1016/j.ijhydene.2025.150980
Received 15 April 2025; Received in revised form 7 August 2025; Accepted 12 August 2025
Available online 28 August 2025

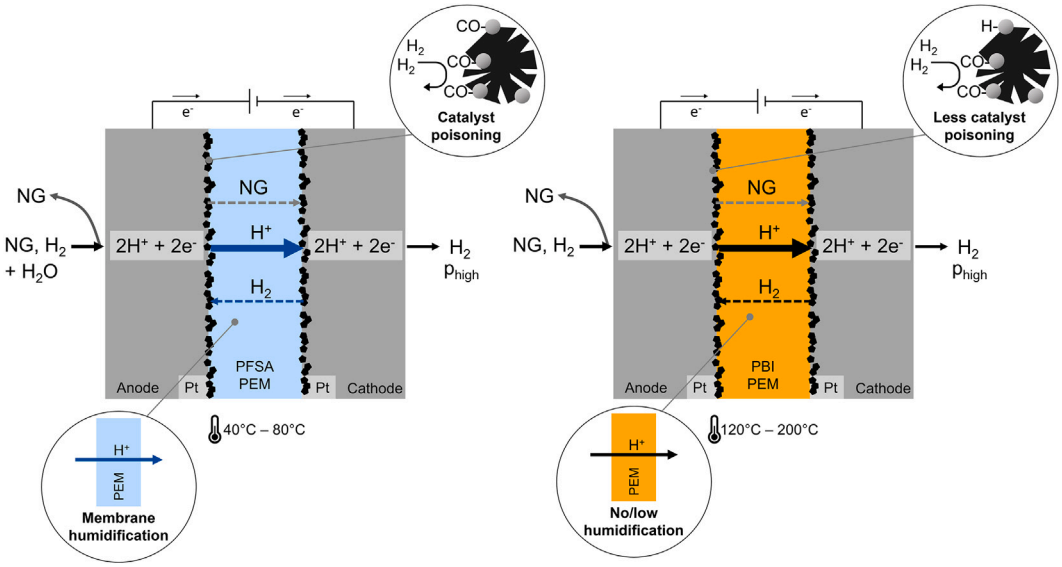

Fig. 1. Working principle of electrochemical hydrogen compression and challenges; NG: Natural gas; PFSA: Perflourosulfonate; PBI: Polybenzimidazole; PEM: Proton exchange membrane.

Table 1
Upper limits of contaminants investigated in this study in the German natural gas grid according to DVGW e.V. technical rule G 260 [14].

Species	Unit	Limit
CO_2	vol.%	4
CO	ppm	100
H_2S	ppm	3.5
NH_3	ppm	14

product gas purity, and stable performance even with detrimental gas impurities in the natural gas [12]. Natural gas mainly consists of methane, propane, butane, carbon dioxide, nitrogen, and oxygen. Additionally, the trace impurities H_2S, CO, COS, mercaptan, silicon compounds, amines, and NH_3 are present, which are among the more critical species for the EHC [13]. The content limits of the contaminants investigated in this study are listed in Table 1.

CO competes with H_2 adsorption and blocks active sites of the platinum catalyst [15]. Adsorption of CO on Pt:

$$Pt + CO \longrightarrow Pt{-}CO \tag{4}$$

Nordio et al. [16] demonstrated that catalyst inhibition from CO_2 is mainly due to reverse water gas shift reaction (RWGS, Eq. (5)) forming CO. Additionally, CO_2 permeating through the membrane can be electrochemically reduced at the cathode of the EHC (Eq. (6)).

$$CO_2 + H_2 \rightleftharpoons CO + H_2O \tag{5}$$

$$Pt{-}CO_{2\,ads} + 2\,H^+ + 2\,e^- \rightleftharpoons Pt{-}CO_{ads} + H_2O \tag{6}$$

H_2S also competes with H_2 for adsorption on Pt (Eq. (7)). Additionally, H_2S dissociates chemically and electrochemically to adsorbed sulfur, forming H_2 or H^+ (Eq. (8), (9)). The complex reaction pathways following H_2S adsorption on platinum can be found in [17–19].

$$Pt + H_2S \rightleftharpoons Pt{-}H_2S_{ads} \tag{7}$$

$$Pt{-}H_2S_{ads} \rightleftharpoons Pt{-}S + H_2 \tag{8}$$

$$Pt{-}H_2S_{ads} \longrightarrow Pt{-}S + 2\,H^+ + 2\,e^-,\ E^0 = 0.165V \tag{9}$$

Contrary to the other listed poisons, NH_3 mainly interacts with the membrane, ionomer, and protons formed in the EHC, reducing the proton conductivity and performance [20–22].

$$NH_3 + H^+ \longrightarrow NH_4^+ \tag{10}$$

In H_3PO_4-doped polybenzimidazole (PBI) based MEAs for high-temperature applications, NH_3 reacts with the acid contained in the membrane to form ammonium salts. This leads to reduced conductivity due to reduced proton activity and mechanical degradation of the membrane [23,24].

$$NH_3 + H_3PO_4 \rightleftharpoons H_2PO_4^- + NH_4^+ \tag{11}$$

For low-temperature, PFSA-based MEAs, ammonia can lead to a loss in conductivity of the membrane and ionomer by substitution of H^+ with NH_4^+, resulting in the ammonium-form of Nafion [20,25].

$$NH_3 + {-}SO^- + H_3O^+ \longrightarrow {-}SO^- + NH_4^+ + H_2O \tag{12}$$

Although CH_4 is considered mostly inert, CH_4 oxidation may occur at the anode of the EHC [26].

$$CH_4 + 2\,H_2O \rightleftharpoons CO_2 + 8\,H^+ + 8\,e^-,\ E^0 = 0.169\ V \tag{13}$$

Table 2 summarizes studies on H_2/CH_4, H_2/natural gas mixtures, and studies on the effect of contaminants in the feed of the EHC. Nordio et al. [16] tested the effect of CO_2 on the EHC and found catalyst inhibition through adsorbed CO from reverse water gas shift. They showed that flushing with air, a so-called air bleed, can quickly recover the inhibited catalyst. Jackson et al. [26] investigated the effect of CO and H_2S on the low-temperature EHC performance and introduced oxygen and ozone dosing as poison mitigation strategies, which oxidize the adsorbed contaminants. After poisoning with 5 ppm H_2S, they achieved up to 98 % recovery of the current density after 20 min ozone cleaning at open circuit potential. In their follow-up study, Jackson et al. [27] fed H_2/CH_4 and H_2/natural gas mixtures to a low-temperature EHC. Even when adding oxidants, they could not achieve stable operation with the H_2/natural gas mixtures. Moreover, the measured product gas purity with H_2/natural gas feed did not reach the ISO 14687-2019-D standard for fuel cells [28]. Mrusek et al. [10] investigated H_2 withdrawal from H_2/CH_4 mixtures in a low-temperature EHC and detected a CH_4 content of 300 ppm in the product gas. Moreover, they investigated the impact of the typically used odorant (THT) on the EHC performance and observed catalyst poisoning by this sulfur compound.

To overcome the aforementioned challenges commonly experienced in low-temperature EHCs, high-temperature EHCs have gained research

Table 2
Overview of studies on poison impact in low and high-temperature electrochemical hydrogen compression, NG: natural gas, PBI: polybenzimidazole; The effect of the respective species on EHC was studied by the following electrochemical technique: CA: chronoamperometry, PC: polarization curve, CP: chronopotentiometry.

Study	Membr.	Effect of CO	CO_2	H_2S	NH_3	NG	Poison **mitigation**	Compr. **and sep.**	Product gas **purity**
Nordio, 2020 [16]	Nafion		CA						
Jackson, 2020 [26]	Nafion	CA		CA			x		
Vermaak, 2021 [21]	TPS	PC	PC		PC				x
Durmus, 2022 [35]	PBI	PC	PC						
Maxwell, 2023 [32]	PBI	PC	PC						x
Jackson, 2023 [27]	Nafion					CP	x		x
Mrusek, 2023 [10]	Nafion							x	
Arunagiri, 2024 [33]	PBI					CP		x	x
Chhetri, 2024 [36]	HTMA-DAPP	CP, PC	PC		PC			x	x
This work	Nafion, PBI	CP, PC	CP, PC	CP, PC	CP, PC		x	x	x

interest. High-temperature EHCs offer a higher tolerance to impurities, improved kinetics and mass transport, and sustainability due to the use of PFAS-free membranes [29]. Additionally, they can operate under anhydrous conditions, enabling more facile process operation [30]. The study of Vermaak et al. [31] presents the separation of H_2 from H_2/CH_4, H_2/CO_2 and H_2/NH_3 mixtures. They employed a H_3PO_4-doped pyridine based aromatic polyether (TPS®) PEM in a high-temperature EHC. During operation with CO_2/H_2 mixtures, a severe decrease in polarization performance was observed due to CO adsorption on the catalyst. When introducing 1500 ppm NH_3 to the EHC, the performance was strongly reduced and broke down completely due to membrane failure with 3000 ppm NH_3. Maxwell et al. [32] introduced H_2/CO_2 mixtures to a high-temperature EHC with a PBI-based PEM. They observed improved polarization performance when operating the EHC at low relative humidity compared to dry operation. Moreover, the current efficiency did not decrease significantly with up to 80 vol.% CO_2 in the feed when operating at 120 °C. Additionally, they identified heating as the main contributor to the EHC's energy demand and showed that waste heat utilization can significantly increase the system's energy efficiency. Arunagiri et al. [33] investigated H_2 withdrawal from natural gas containing 10 % H_2 using a high-temperature PEM and binder and observed a degradation rate of 44 µV h^{-1} in a 100 h test. However, their gas did not contain H_2S or CO, which are expected to be among the most critical impurities in the natural gas grid [13,33].

To date, no study has systematically compared low- and high-temperature EHC performance when operating with trace impurities present in natural gas, enabling a critical review of which technology is suitable for the application. Additionally, poison mitigation strategies, apart from dosing oxidants, which can cause PEM-degradation by H_2O_2 and subsequent radical formation, have been neglected in literature for EHC [34]. Our work compares the performance and operation window of the low- and high-temperature EHC in the same test cell as a benchmark. The effects of H_2S, CO, CO_2, and NH_3 on the EHC's performance are systematically investigated, and operation strategies to mitigate the effects of these gas impurities are tested for their suitability for EHC operation.

2. Material and methods

30 % hydrogen peroxide was purchased from Sigma-Aldrich Chemie GmbH (GER), and 2.5 mol L^{-1} sulfuric acid was purchased from VWR International (USA). All chemicals were used as received. 8 vol.% CO_2 blended with H_2 and N_2 5.0 was supplied from Westfalen AG (GER), 8 ppm H_2S in H_2, 60 ppm CO in H_2, H_2 5.0 and Ar 4.8 from Air Products and Chemicals (USA). 28.5 ppm NH_3 in H_2, CH_4 4.5 and synthetic air were obtained from Taiyo Nippon Sanso Corporation (JP). Ultra-pure water was used with a conductivity of less than 0.05 mS cm^{-1} (Milli-Q® (Merck KGaA, GER)).

Nafion 117 was supplied from DuPont de Nemours (USA) with a dry thickness of 180 µm. Gas diffusion electrodes with 0.5 mg cm^{-2} Pt loading on Sigracet 29BC (SGL Carbon SE, GER) carbon paper (thickness: 250 µm) and BASF Celtec-P1200 W MEA (BASF SE, GER) MEAs with 1 mg cm^{-2} Pt loading on one and 0.7 mg cm^{-2} Pt loading on the other electrode with an active area of 25 cm^2 were acquired from Quintech (GER). The electrode with the 0.7 mg cm^{-2} Pt loading was used as the anode in this study.

2.1. Low-temperature MEA preparation

The Nafion 117 membrane was activated before MEA fabrication following the protocol given in the supplementary information. Before hot pressing, excess water was removed from the membranes by blow drying. Two 5×5 cm Sigracet 29BC GDEs were placed on both sides of the membrane, and the assembly was sandwiched between a 1 mm thick PTFE flat sheet and aluminum foil to prevent imprinting during hot pressing. This stack was hot pressed at 130 °C for 2 min and then at room temperature for 1 min with 20 bar hydraulic pressure in a Polystat 300 S2 (Servitec Maschinenbau GmbH, GER) press. The Nafion MEAs were stored at room temperature at 100 % relative humidity (RH) until further use.

2.2. Test cell

A Flex-E-Cell (FXC Engineering GmbH, GER) was used as the EHC. Figure S1 depicts the cell assembly without backplates and bolts used in the electrochemical experiments. The bipolar plates had a parallel flow channel design with an active area of 25 cm^2. Both the inlet at the top and the outlet at the bottom were equipped with flow dividers to uniformly distribute the gas. For the Nafion-MEAs, the bipolar plates were made of gold-plated stainless steel (SS), and Celtec-MEAs used titanium bipolar plates. The contact pressure was adjusted using Fujifilm Prescale LLW-LW (FUJIFILM Europe GmbH, GER) pressure indicator film to approximately 2 MPa. The four bolts of the cell were tightened with a torque wrench to 20 N · m.

2.3. Experimental setup

Fig. 2 shows the flow sheet of the experimental setup used for the electrochemical experiments. Serie 35 831MLW (Analyt-MTC, GER) mass flow controllers (MFC) regulated the volumetric flow of all gases supplied to the EHC. The hydrogen supply stoichiometry in the manuscript is described by λ, which is defined by the quotient of the supplied amount of H_2 and the theoretical necessary supply of H_2.

$$\lambda = \dot{n}_{H2,in}/\dot{n}_{H2,theor} \quad (14)$$

The back pressure on the cathode side was regulated by a spring-loaded back pressure regulator (Swagelok, USA) if required and monitored via a pressure transducer (A-10, WIKA, GER). Gas flowed either through a controlled evaporation mixer (CEM, W-102 A, Bronkhorst High-Tech B.V., NL), a humidification bath, or bypassed the humidifiers to purge the anode and cathode compartments. The humidifier bath was used

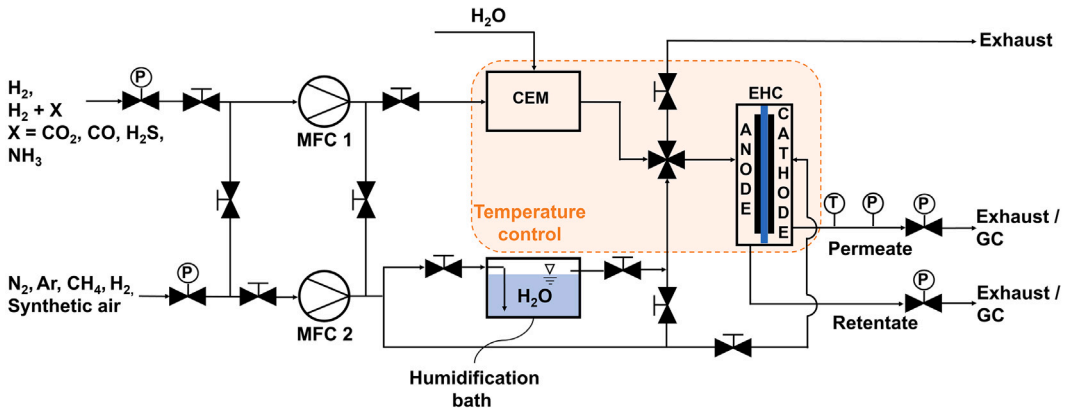

Fig. 2. Experimental setup.

for humidities below the operation range of the CEM. When using the humidification bath, the humidity was regulated by mixing the gas exiting the humidifier with dry gas. The CEM, capillaries between CEM and EHC, and the EHC were heated electrically. The capillaries were heated by an HS 450 °C wire heating system, and the cell by a 400 W custom-made two plate heating system (HORST GmbH, GER) and controlled by an HT MC11 (HORST GmbH, GER) temperature controller. All heated parts were insulated. Data was collected with an echem-workstation and software (ZUMOlab GmbH, GER).

2.4. Electrochemical experiments and analytics

The electrochemical experiments were performed using a VSP potentiostat with a 20 A VMP3B-20 booster (BioLogic, USA) controlled by the EC-Lab software (BioLogic, USA). The cell was connected by 4 mm diameter banana plug connectors attached to each bipolar plate in a two-electrode configuration. For experiments above 70 °C, an additional set of high-temperature banana plugs was inserted between the booster and cell. Depending on the current density, these plugs add an additional ohmic resistance of 0.5 mΩ to 1 mΩ, which was not corrected in the data analysis. Each MEA was preconditioned when used for the first time according to the protocol in Table S1. The protocol for the benchmark characterization is given in Table S2.

The current steps for the benchmark characterization were set to 0.25 A and 15 %, 30 %, 45 %, 60 %, 70 %, 80 %, and 90 % of the limiting current. Unless otherwise stated, electrochemical impedance spectrum (EIS) measurements were performed in a frequency range of 100 kHz to 1 mHz with 8 points per decade and an amplitude of 40 % of the DC current or cell potential while taking the average of three measurements per frequency. Electrochemical impedance spectra measurements were conducted at 50 mV or 0.1 A cm^{-2}, respectively.

The electrochemically active surface area (ECSA) was determined via the hydrogen adsorption and desorption method [37,38]. To determine the ECSA, the potential is cycled between 0.02 V to 0.6 V at a scan rate of 35 mV s^{-1} unless otherwise noted. A minimum of five cycles are performed until the CV is stable. The CV measurements are performed with dry gas at a flow rate of 25 mL min^{-1}. The last cycle is used to determine the ECSA according to Eq. (15) by manual integration of the respective areas (A_{ads}, A_{de}) in EC-Lab and with the specific oxidation charge $q_{Pt} = 210\,\mu C\,cm^{-2}$ [37].

$$\text{Area per area of GDE: } ECSA = 0.5 \cdot \frac{A_{ads} + A_{de}}{q_{Pt} \cdot Scanrate} \tag{15}$$

Gas compositions were obtained by gas chromatography with an Agilent 8860 GC system (Agilent Technologies, Inc, USA). The carrier gas was helium at a flow rate of 5.7 mL min^{-1}. The fuel gas stream was composed of 350 mL min^{-1} synthetic air and 35 mL min^{-1} H_2. A molecular sieve column 5 A 80/100 mesh (Agilent Technologies, USA), a Haysep Q micro column HysepQ 80/100 mesh (Agilent Technologies, USA), and a PoraBOND Q column (Agilent Technologies, USA) were installed as separation columns.

2.5. Efficiency

The energy efficiency $\eta_{E,Energy}$ of the EHC was calculated by dividing the output energy as the energy content of the product gas minus the energy consumed by the EHC by the energy content of the H_2 input and the energy for heating ($\dot{Q}_{Heating}$) assuming the availability of waste heat [32]. The energy content of H_2 was calculated using the higher heating value (HHV) and the molar product flow of hydrogen ($\dot{n}_{H2}$). The energy consumed was calculated by the product of the cell potential (E_{cell}), the current density (j), and the geometrical area of the electrodes (A). The electric power (P_{el}) of the heating unit is given in Table S3.

$$\eta_{E,Energy} = \frac{\dot{n}_{H2} \cdot HHV_{H2} - E_{cell} \cdot j \cdot A}{\dot{n}_{H2} \cdot HHV_{H2} + \dot{Q}_{Heating}} \tag{16}$$

The energy required for heating, assuming a waste heat source, was calculated based on the electrical heating power measured in the test stand and the environment (T_u) and EHC operating temperature (T_{EHC}) [32].

$$\dot{Q}_{Heating} = P_{el} \cdot (1 - T_U / T_{EHC}) \tag{17}$$

Assuming 100 % faradaic efficiency and neglecting $\dot{Q}_{Heating}$ the generalized ideal definition of the voltage efficiency is derived as in Eq. (18), where 1.483 V results from the division of HHV_{H2} by $2F$:

$$\eta_{E,Voltage,ideal} = 1 - \frac{E_{cell}}{1.483\ [V]} \tag{18}$$

2.6. Poisoning and poison mitigation

Table S4 lists the procedure for the poisoning experiments. The flow rates of the gases in the feed gas mixture are summarized in Table S5. Before the contaminants are introduced into the system, measurements are denoted as BoT (Beginning of Test) and afterward as EoT (End of Test). Data obtained after performing a mitigation strategy are labeled according to the strategy.

Before the recording of the BoT measurements, the EHC was operated at the experimental conditions, without the contaminant, at 400 mA cm^{-2} until the change in potential was less than 1 μV s^{-1}. A new MEA was used for each contaminant. For H_2S contamination, three CV oxidation cycles were added before the test procedure to remove residual H_2S. ECSA, electrochemical impedance, and polarization were recorded at BoT (Fig. 3 (0)), EoT (Fig. 3 (4)), and after mitigation. After measuring the BoT, the system was run at 500 mA cm^{-2} with pure H_2 feed for a minimum of 30 min until the change of potential was less than 1 μV s^{-1}. However, only the last 30 min will be shown in the data. The contaminants were then fed to the EHC for 3.5 h or the mentioned time (Fig. 3 (1–2)). Then, the feed was switched back to pure H_2 for 15 min (Fig. 3 (2–3)) and then back to the contaminant for the remainder of the

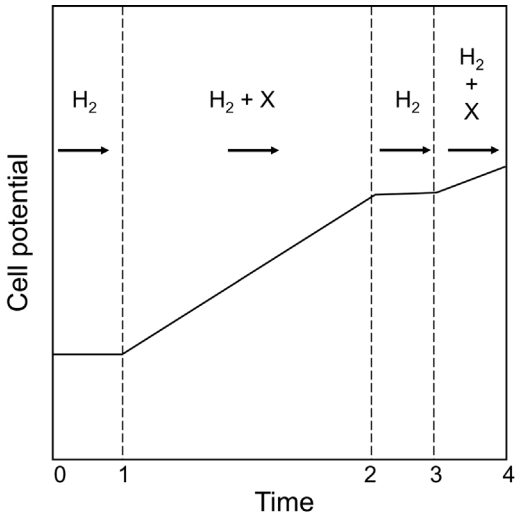

Fig. 3. Illustration of the experimental procedure for the poisoning experiments. 0 – 1: Operation with pure H_2, 1 – 2: Operation with respective poison; 2 – 3: Operation with pure H_2; 3 – 4: Operation with respective poison; vertical dashed lines indicate the change of gas composition.

measurement to verify the observations (Fig. 3 (3–4)). Afterward, EoT was measured (Fig. 3 (4)). Then, the mitigation strategy was performed. The following mitigation strategies were employed. For air bleeding, synthetic air was introduced for 90 s at a rate of 150 mL min^{-1}. Before and after the air bleed, the cell was flushed with N_2 for 30 s at the same flow rate. For cyclic oxidation, five CV cycles were performed in the potential window of 0.02 V to 1.2 V at a scan rate of 35 mV s^{-1}. When performing cyclic heating, the cell was repeatedly heated to 160 °C, then switched off until the base temperature of 120 °C was reached.

2.7. Uncertainties

The temperature of the cell was controlled with a deviation of ±0.15 °C. The gas mixtures with impurities were supplied as pre-mixed gases with ±2 rel.% accuracy for CO, CO_2 and NH_3 and ±5 rel.% accuracy for H_2S and analysis certificate. Considering the precision of the mass flow controllers and the accuracy of the pre-mixed gases, the compositions of the feed gas mixtures in the poisoning experiments are 4±0.18 vol% CO_2, 30±1.5 ppm CO, 14±0.7 ppm NH_3 and 3.5±0.3 ppm H_2S. These uncertainties in gas composition are minimal and expected to have no significant influence on the observations reported [39,40]. Gas compositions determined with gas chromatography were determined as the mean value of two samples. Each sample was measured twice. The deviation of the measurements is presented as error bars. The accuracy of the 4-point calibration was $R^2 = 0.99992$. The hydrogen underpotential deposition method used to determine the ECSA has an accuracy of ±10 % [38,41]. The relative deviation in polarization after conditioning was within 1 % for the low-temperature MEAs (n = 2, k = 1) and 8 % for the high-temperature MEAs (n = 4, k = 1) used in this study. The poisoning experiments, except for the 16 h and 75 h experiments, were repeated twice. The mean value of the relative increase in cell potential, including the standard deviation, is presented in a summary table (n = 2, k = 1).

3. Results and discussion

3.1. Benchmark characterization

A low-temperature EHC with Nafion 117 MEA (Nafion-EHC) and a high-temperature EHC with Celtec-P1200 W MEA (Celtec-EHC) were characterized with pure H_2 to establish a benchmark for the poisoning investigations. The current density of the Nafion-EHC at 50 mV in Fig. 4 (a) rises with increasing temperature from 20 °C to 70 °C while the high-frequency resistance (HFR) decreases. The achieved current is in good agreement with literature using the same membrane [42,43]. For the Celtec-EHC with dry feed gas (Fig. 4 (a)), the current density increases from almost zero at 20 °C, with increasing slope until 120 °C, where it reaches similar values to the Nafion-EHC and no significant increase in current is observed when increasing the temperature further. The HFR of the Celtec-EHC, dominated by the resistance of the proton exchange membrane, decreases steeply until 70 °C. The conductivity of acid-doped PBI increases with increasing temperature following the Arrhenius equation [44]. This behavior is also reported by the manufacturer data. When increasing the feed gas relative humidity, the achieved current density rises by 90 mA cm^{-2}.

The dry Celtec and Nafion-EHC show a linear polarization behavior until 600 mA cm^{-2}, with similar performance, as shown in Fig. 4 (b). At current densities above 600 mA cm^{-2}, the Nafion-EHC shows non-linear behavior, which is more pronounced when iR-corrected and could be attributed to water mass transport limitations leading to drying [42,45,46]. The humidified Celtec-EHC achieved about 30 % lower cell potential than in dry operation, and a linear polarization behavior is observed for the investigated current range. This improvement in cell potential can be attributed to an increased proton conductivity of the PEM, caused by phosphoric acid dissociation induced by water [47]. Additionally, the increased humidity improved the stability of the operation of the MEA, presumably by suppressing the hydrolysis of phosphoric acid at high temperatures [44]. In the dry operation of the Celtec-EHC at constant current, shown in Fig. S2, a potential increase over time was observed, which was more pronounced at increased temperatures. For the Celtec-EHC, the potential in the iR-corrected polarization curves at 0 % and 10 % RH is close to 0 mV, indicating mostly iR-losses in the cell.

Compression of pure H_2 was investigated until 6 bar cathode pressure, see Fig. 4 (c). The graph shows the cell potential, the iR-corrected cell potential, and the compression efficiency, which is calculated by dividing the Nernst potential by the measured potential at different cathode pressures. The compression efficiency of the Celtec-EHC was generally higher than that of the Nafion-EHC due to the lower cell potentials achieved. At a cathode pressure of 6 bar, the compression efficiency was slightly above 40 % for the Celtec and 30 % for the Nafion-EHC.

The purification of H_2 from 50/50 and 80/20 vol.% CH_4/H_2 mixtures was investigated. The CH_4 content in the product gas, shown in Fig. 4 (d), is higher with increasing CH_4 feed content and decreasing current density. With a higher CH_4 share in the feed, the partial pressure difference and thus driving force for CH_4 gas permeation increases, leading to a higher diffusion rate. While this phenomenon is independent of current density, H_2 evolution is driven by current density. Thus, high current densities favor high purities. The CH_4 content in the product gas is one order of magnitude higher for the Nafion-EHC, indicating a higher gas permeability of the Nafion membrane. For example, the H_2 permeability is one order of magnitude larger for Nafion 117 with $5 \cdot 10^{-11}$ molcm^{-1}s^{-1}bar^{-1} at 70 °C [48] than for H_3PO_4-doped PBI with $7.7 \cdot 10^{-12}$ molcm^{-1}s^{-1}bar^{-1} at 160 °C [49]. When increasing the operating temperature of the Celtec-EHC from 120 °C to 160 °C, the CH_4 content increases, which can be explained by increased gas permeability at higher temperatures due to increased diffusivity [50].

3.2. Impact of CO_2 or CO in H_2 on the EHC performance

To differentiate the effect of the contaminants in NG, mixtures of H_2 and single poisons were introduced to the EHCs. All experiments started with pure H_2 feed for 30 min. Furthermore, the feed was switched back to pure H_2 from 240–255 min to validate the observations. The cell

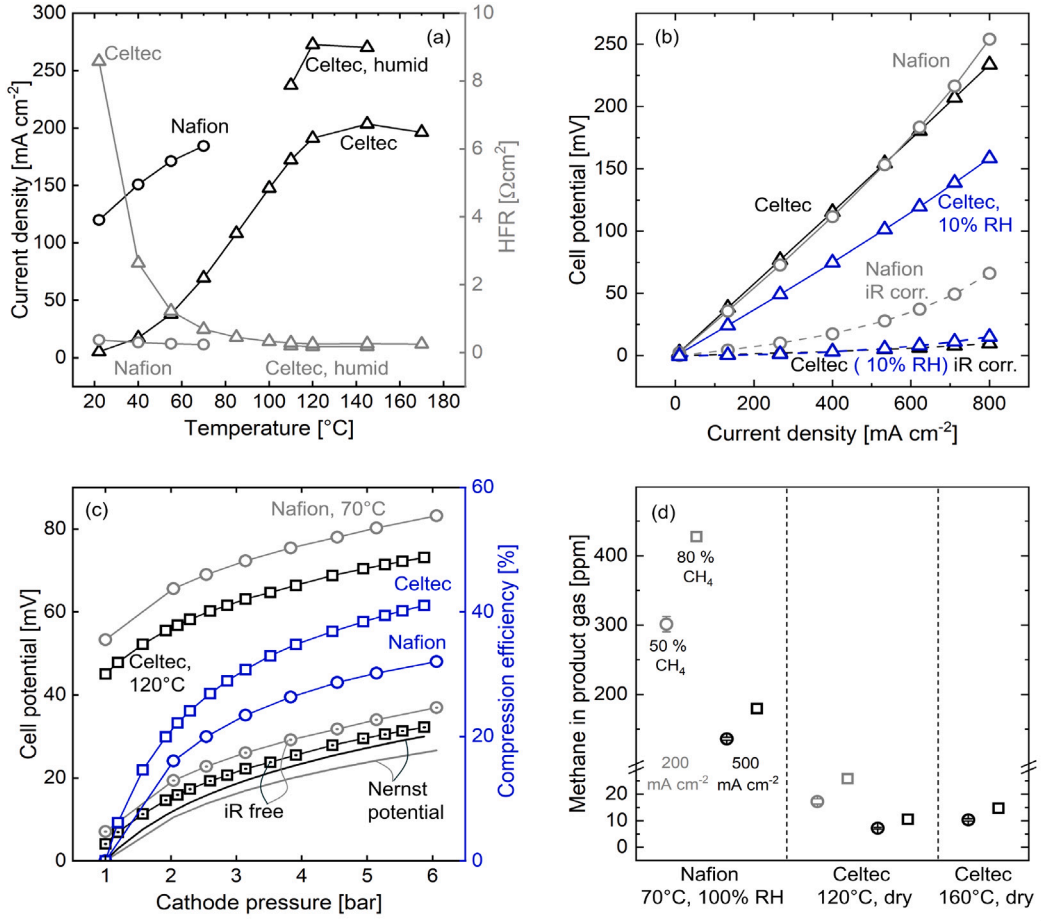

Fig. 4. (a) Average current density at 50 mV (black) and high-frequency resistance (HFR, grey) of EHC with Nafion 117 at 100 % RH (circles) and Celtec MEA dry and Celtec MEA humid with 2.4 g h^{-1} water in the 200 mL min^{-1} feed gas (triangles); (b) Polarization curve from current steps of EHC with Nafion 117 (circles, grey) at 100 % RH and 70 °C and Celtec MEA at 0 % (black) and 10 % (blue) RH and 120 °C, (c) Cell potential and compression efficiency at different cathode pressures, (d) Purity of H_2 when separated from H_2/CH_4 mixtures.

potential of the Nafion-EHC, presented in Fig. 5 (a), increases for 3 h upon introduction of 4 vol.% CO_2 until stabilizing at 180 mV, which is a 35 mV increase in cell potential compared to the BoT. The potential does not recover when switching the feed stream back to pure H_2. When CO_2 is introduced to the Celtec-MEA, the cell potential increases by 3 mV and drops by 2 mV once switching back to pure H_2. The EoT polarization curves (Fig. S3 (a)) show a 20 % increase in the potential for the Nafion-EHC and a 3 % increase for the Celtec-EHC (Fig. S4 (a)), which is also observed in the iR-corrected polarization curve, indicating that the increased potential is mainly caused by deteriorating charge or mass transfer. With 4 % CO_2, an increase of 0.6 mV to 0.7 mV would be expected from the Nernst equation, depending on the operating temperature. The charge transfer resistance of the Nafion-EHC in the EoT EIS strongly increases (Fig. 5 (c)), while no significant changes are observed for the Celtec-EHC. The potential and charge transfer resistance increase can be attributed to catalyst poisoning by CO_2 and CO, formed by RWGS (Eq. (5)), adsorption on the Pt active sites, decreasing the active catalyst surface for the HOR [16,35].

The ECSA of the electrodes was determined before and after the poisoning experiments. A reference experiment with H_2 and CH_4 showed an ECSA reduction of 3.6 % for the anode and 5.8 % for the cathode (Fig. S5 (b)). The ECSA was determined using the last of at least five cycles; consequently, changes in ECSA due to oxidation of adsorbed species in prior cycles are undetected. The ECSA analysis could not be performed for CO_2 because most of the adsorbed CO was oxidized in the 'pre-peak' region below 0.6 V (Fig. S6 (a)) [51]. However, in the CV of the anode at EoT, a reduced hydrogen oxidation charge (0.1 V to 0.3 V) can be qualitatively observed (Fig. S6 (a)). The oxidation peak in the CO-stripping region can also be observed in the CV of the cathode in Fig. S6 (b), indicating that CO_2 crossover by permeation to the cathode side occurs and CO is formed by electroreduction of CO_2 (Eq. (6)). Consequently, the cathode catalyst is also poisoned by CO leading to a reduction in active sites for HER as indicated by the reduced hydrogen oxidation charge in the CV of the cathode side (Fig. S6 (b)). For the Celtec-EHC, a more severe decrease of the anode ECSA of 12 % was measured (Fig. S5 (b)), which can be caused by increased CO formation from the RWGS at higher temperatures and low humidity. For the Celtec-EHC, no CO oxidation peak was observed at potentials below 0.6 V (Fig. S7 (a), (b)).

With 30 ppm CO in the feed stream, the cell potential of the Nafion-EHC, shown in Fig. 5, rises steeply for the first 30 min and then increases until stabilizing after about 3 h at 380 mV (Fig. 5 (b)). At controlled current operation, an equilibrium between CO adsorption and oxidation is maintained, leading to operation at elevated potentials [52,53]. In contrast, Jackson et al. [26], operating the EHC with Pt-catalyst at controlled potential, observed a detrimental reduction in current density exceeding 90 % after 30 min, as the operating potential (200 mV) was below the oxidation potential of CO. When switching back to H_2, the potential drops steeply but immediately jumps back to 380 mV when CO is reintroduced. This stark change can also be observed

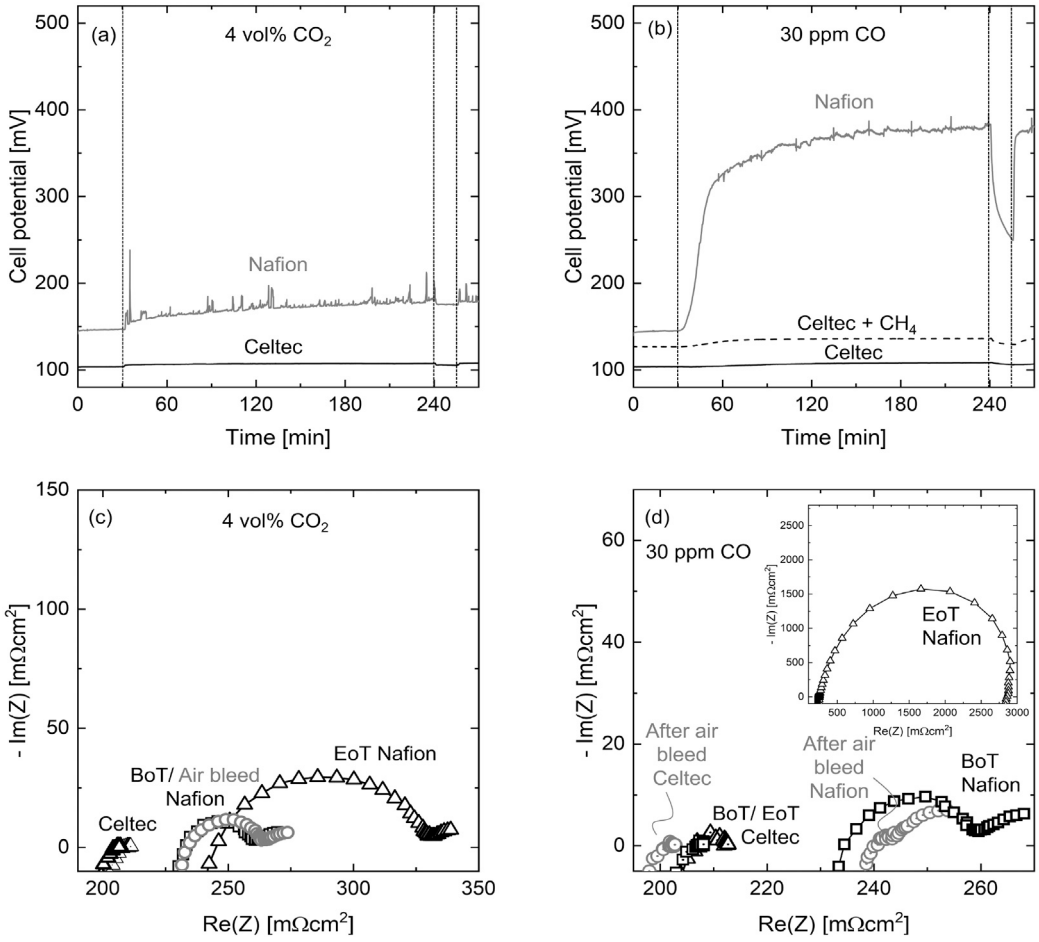

Fig. 5. (a) Cell potential over time when adding 4 vol.% CO_2 to the EHC feed, no poison was introduced for the first 30 min and from 240–255 min, vertical dashed lines indicate the change of gas composition, 500 mA cm^{-2}, λ = 1.6, Nafion-EHC: 70 °C, 100 % RH; Celtec-EHC: 120 °C, 0.7 % RH; (b) Cell potential over time when adding 30 ppm CO to the EHC feed, no poison was introduced for the first 30 min and from 240–255 min, vertical dashed lines indicate the change of gas composition, 500 mA cm^{-2}, λ = 1.3 for CO; Nafion-EHC: 70 °C, 100 % RH; Celtec-EHC 120 °C, 0.7 % RH; dashed line: Impact of 30 ppm CO, when feed stream is diluted with 50 vol.% CH_4, λ = 1.6; Electrochemical impedance spectra with (c) 4 vol.% CO_2 or (d) 30 ppm CO Beginning of Test (BoT): squares, End of Test (EoT): triangles, after air bleed: grey circles.

in the charge transfer resistance semi-circle in the EIS analysis (Fig. 5 (d)), which is significantly enlarged at EoT. For the Celtec-EHC, the potential rises with decreasing slope by 4 mV over 3.5 h (Fig. 5 (b)). The poisoning effect of CO is less severe for the Celtec-EHC because the equilibrium surface coverage of CO on the Pt catalyst is reduced with increased temperature [13]. Additionally, HER and HOR kinetics are faster at increased temperatures, and the Celtec-EHC has a higher catalyst loading. When adding 50 vol.% CH_4 to the feed of the Celtec-EHC, the potential increases by 11 % (Fig. 5 (b)). In the Nafion-EHC EoT polarization curve (Fig. S3 (b)), a jump in potential of 200 % increase is observed from 100 mA cm^{-2} on. The potential remains at the oxidation potential of CO, indicating a high catalyst surface coverage with CO. An increase of 4 % is observed in the EoT polarization curve of the Celtec-EHC (Fig. S4 (b)). The ECSA of the Celtec-EHCs anode decreased by 24 % with CO (Fig. S5 (b)). The performance was restored for both cells by an air bleed after poisoning with CO_2 or CO.

In summary, adding 4 vol.% CO_2 or 30 ppm CO to the feed gas strongly impaired the Nafion-EHC performance, while for the Celtec-EHC, a minimal increase in cell potential was observed.

3.3. Impact of NH_3 in H_2 on the EHC performance

After the addition of 14 ppm NH_3 to the feed of the EHC, a slight increase in cell potential slope (1 mV h^{-1}) can be observed for the Nafion-EHC, in Fig. 6 (a), compared to the reference experiment without poison (0.32 mV h^{-1}). Fig. 6 (b) shows the EIS analysis of the Nafion-EHC before and after poisoning. The EoT measurement shows an increase in HFR and charge transfer resistance. The increased HFR and charge transfer resistance might be attributed to reduced ionomer conductivity by ion exchange to the NH^+ form of Nafion [25]. However, the effect observed herein of adding 14 ppm NH_3 is less severe than reported in the literature by Halseid et al. [54] for a Gore MEA at 40 °C, which might be due to the higher operating temperature and the thicker membrane used in our study [55]. No significant changes in cell potential (Fig. 6 (a)), polarization behavior (Fig. S4 (d)) or ECSA (Fig. S9) can be observed for the Celtec-EHC during the 3.5 h poisoning experiment with 14 ppm NH_3, also when diluted with CH_4 (Fig. 6 (d)). When operating the Celtec-EHC for 15 h with 14 ppm NH_3, as presented in Fig. 6 (c), a potential increase rate of 55.8 µV h^{-1} was measured. However, Huang et al. [56] observed an increase of about 130 µV h^{-1} with an H_3PO_4-doped m/p-PBI membrane when operating without any poison at 120 °C. Consequently, the increase in potential could also be attributed to degradation mechanisms non-related to NH_3 or run in.

To challenge the Celtec-MEA for long-term operation stability when introducing NH_3, a long-term test for 75 h alternately introducing H_2 with 14 ppm NH_3 and pure H_2 for 12 h was performed (Fig. 6 (c)). For the periods with a pure H_2 feed, the potential declines with an

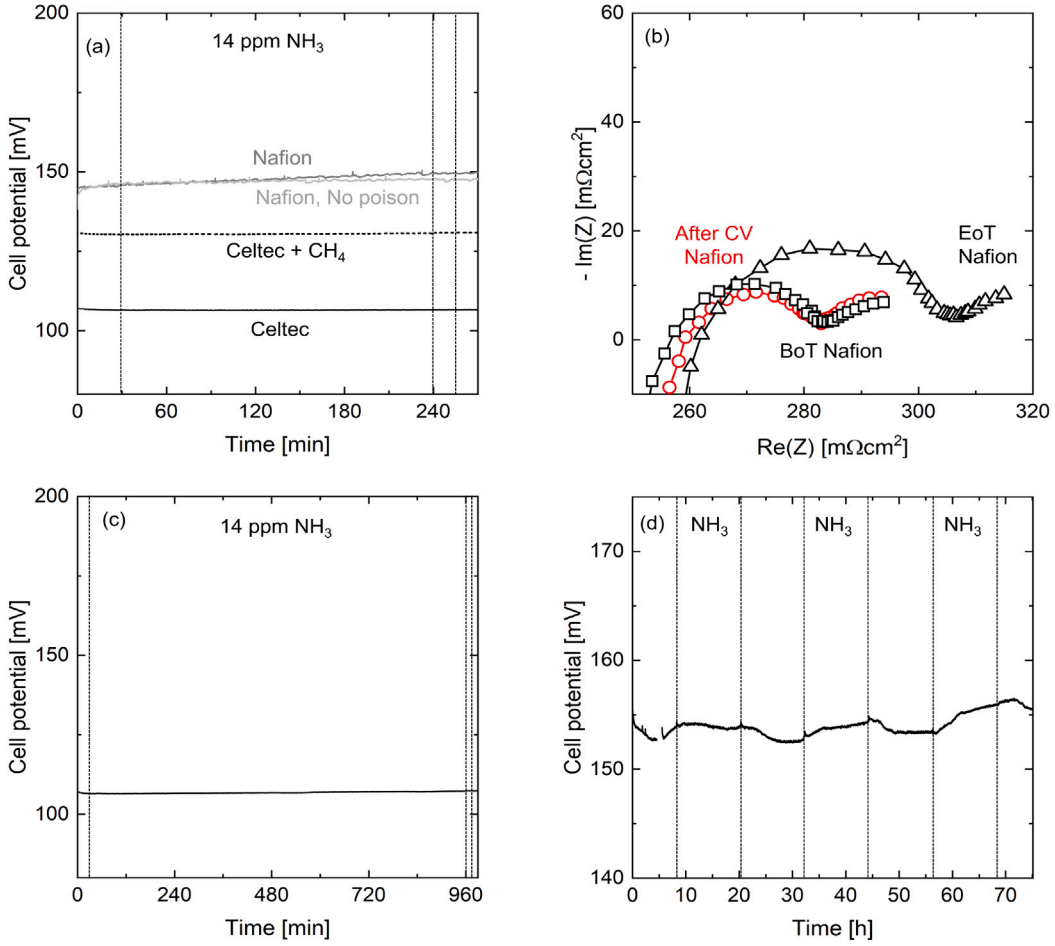

Fig. 6. (a) Cell potential over time when adding 14 ppm NH_3 to the EHC feed, no poison was introduced for the first 30 min and from 240–255 min, vertical dashed lines indicate the change of gas composition, 500 mA cm^{-2}, λ = 1.3; dashed line: Impact of 14 ppm NH_3, when feed stream is diluted with 51 vol.% CH_4 (dashed lines), λ = 1.6; Nafion-EHC: 70 °C, 100 % RH; Celtec-EHC: 120 °C, 0.7 % RH; (b) Electrochemical impedance spectra of Nafion-EHC with 14 ppm NH_3, Beginning of Test (BoT): squares, End of Test (EoT): triangles, after air bleed: grey circles, after CV cleaning: red circles; (c) Cell potential over time a Celtec-EHC when adding 14 ppm NH_3 to the EHC feed, no poison was introduced for the first 30 min and from 960–975 min, 500 mA cm^{-2}, λ = 1.3, 120 °C, 0.7 % RH; (d) Cell potential of a Celtec-EHC when alternately introducing H_2 with 14 ppm NH_3 and pure H_2 for 12 h each, 120 °C, 0.7 % RH, λ = 1.3.

average slope of −83 µV h^{-1} while during the periods with NH_3 the potential increases by 124 µV h^{-1}. Although no change in potential was measured in the 3.5 h poisoning experiment, these observations indicate an adverse long-term effect of NH_3 on the Celtec-EHC, which could be caused by the reduction of the membrane conductivity by the interaction of NH_3 with H_3PO_4 (Eq. (10)). The long-term adverse effect of NH_3 has been reported for fuel cells with PBI-based MEAs [24]. To confirm that the potential increase is caused by NH_3, more extended poisoning experiments >200 h focusing on the ionomer and membrane conductivity should be conducted in future research to elucidate the effect of NH_3 on Celtec-EHCs and differentiate the increase caused by NH_3 from other degradation mechanisms.

Even though the charge transfer resistance increased, the change in cell potential after 3.5 h NH_3-poisoning in the Nafion-EHC was minimal. This can be explained by the HFR dominating the cell potential, which increased after poisoning, but only minimally. After CV-cleaning, the charge transfer resistance and the HFR decrease. Consequently, CV-cleaning mitigates NH_3 poisoning; however, it is unclear whether the poisoning is completely reversible.

3.4. Impact of H_2S in H_2 and H_2/CH_4 mixtures on the EHC performance

When introducing 3.5 ppm H_2S to the Nafion-EHC, the cell potential starts increasing 30 min after the poison is introduced and then rises linearly until it reaches 480 mV after 3.5 h. Even when the feed is switched back to pure H_2, the cell potential continues to increase, as shown in Fig. 7 (a). The charge transfer resistance semi-circle in the EoT EIS analysis increased (Fig. 7 (c)). For comparison, the poisoning rates of other manuscripts investigating poisoning under galvanostatic conditions and our experiments are summarized in Table S6. Jackson et al. [27] observed an increase of cell potential to 1.4 V after 2.5 h operating a low-temperature EHC at 35 °C with 50 % H_2 in NG containing 0.78 % CO_2 and 1.8 ppm volatile sulfur compounds. Mrusek et al. [10] observed a similar trend when introducing the sulfur-containing odorant THT to a low-temperature EHC. We could not observe the exponential increase in cell potential for the low-temperature EHC operating with CO or H_2S during the conducted four-hour poisoning as in Jackson et al. [27]. Our feed gas contained H_2S or CO, and it is reported in literature that poisoning with a mixture of H_2S and CO is more severe than one poison alone [15,57]. Additionally, the higher total poison concentration, lower operation temperature and the dilution of hydrogen with natural gas can justify the more severe poisoning in the study of Jackson et al. [27].

The cell potential of the Celtec-EHC increases by 1 mV throughout the poisoning experiment with H_2S (Fig. 7 (a)), and no significant change can be observed in the EIS analysis (Fig. 7 (d)). The potential in the EoT polarization curve increased by 267 % for the Nafion-EHC (Fig. S3 (d)). For the Celtec-EHC, no significant change in polarization behavior was observed in the 3.5 h poisoning test (Fig. S4 (c)). The ECSA

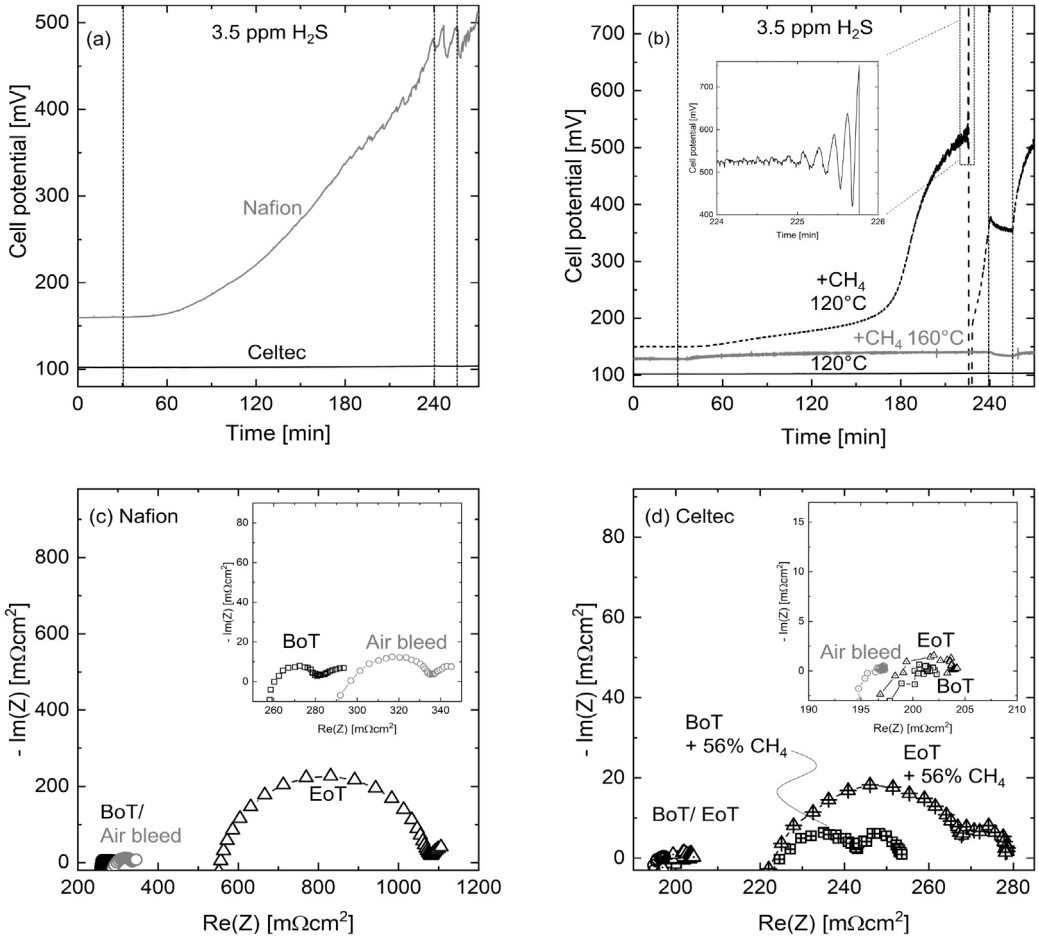

Fig. 7. (a) Impact of 3.5 ppm H_2S on EHC performance, no poison was introduced for the first 30 min and from 240–255 min, vertical dashed lines indicate the change of gas composition, 500 mA cm^{-2}, λ = 1.3; Nafion-EHC: 70 °C, 100 % RH; Celtec-EHC 120 °C, 0.7 % RH; (b) Impact of H_2S when feed stream is diluted with CH_4, no poison was introduced for the first 30 min and from 240–255 min, λ = 1.6 H_2S 56 vol.% CH_4, grey line: 160 °C, 2.1 % RH ; Electrochemical impedance spectra, (c) of a Nafion 117 MEA with 3.5 ppm H_2S BoT: squares, EoT: triangles, after air bleed: grey circles; (d) of a Celtec MEA with 3.5 ppm H_2S BoT: squares, EoT: triangles, after air bleed: grey circles with 3.5 ppm H_2S and 56 vol.% CH_4 (symbols with cross).

of the Nafion-EHC anode, presented in Fig. S10, decreased by 80 % at EoT while the ECSA of the Celtec-EHC anode decreased by 21 % at EoT.

However, when performing a 15 h experiment with H_2S in the Celtec-EHC, shown in Fig. 8 (a), a 12 % increase in cell potential over 15 h operation with H_2S was observed. Additionally, an increase in the HFR and charge transfer resistance after poisoning (EoT) was observed in the impedance spectra in Fig. 8 (b). This indicates a long-term poisoning effect of H_2S in the Celtec-EHC operating at 120 °C. Consequently, longer operation with H_2S should be investigated in future work. Additionally, developing accelerated aging protocols when operating with poisons would facilitate future research in this field.

When diluting the H_2/H_2S feed stream of the Celtec-EHC with CH_4 (Fig. 7 (b)), the cell potential increases linearly for about 150 min, reaching 200 mV. Subsequently, the potential increases exponentially for approximately 30 min until the slope decreases, while potential oscillations can be observed. The amplitude of the oscillations increases until a potential spike to the potential limit of the potentiostat occurs after about 225 min, after which the cell potential drops and the process of potential increase and oscillations is repeated. With the diluted H_2S/H_2 feed stream, an increased HFR and charge transfer resistance compared to the non-diluted feed can be observed in the impedance spectrum at BoT and EoT (Fig. 7 (d)). Additionally, a second semi-circle indicating mass-transport limitation was measured. At EoT, the charge transfer resistance increases compared to BoT, indicating catalyst poisoning and a disrupted proton conduction path. The ECSA with diluted H_2S/H_2 feed decreases by 25 % compared to BoT, which is 5 % more compared to the undiluted feed (Fig. S10). Possibly, even more severe ECSA reduction from sulfur poisoning occurred during the poisoning experiment, but high cell potentials during the self-oxidation cycles probably led to partial oxidation of the adsorbed sulfur species, thereby recovering the catalyst area.

The detrimental effect upon dilution can be explained by the poisoning mechanisms of H_2S. H_2S dissociates to S and H_2 when adsorbing to Pt (Eq. (8)). Consequently, with decreased H_2 share in the feed, the adsorption equilibrium is shifted towards S adsorption. The significant increase in cell potential after 150 min may be induced by the start of electro-oxidation of H_2S, which has a thermodynamic equilibrium potential of 165 mV [19]. Pt–S interferes electrostatically with the adjacent active sites, and the electrochemical dissociation may hinder the backreaction of Pt–S to H_2S and Pt because the intermediate of the reaction (Pt–H_2S) is electrochemically oxidized [58]. The potential spike may be caused by severe catalyst poisoning, which leads to an increase in cell potential until the oxidation potential for S is reached. The oxidation onset potential for sulfur oxidation to SO_2 at 70 °C is between 500 mV to 600 mV vs. DHE [17]. The polarization curve displayed in Fig. S4 (e) shows a strong potential dependence on the poisoning. Between 200 mA cm^{-2} to 300 mA cm^{-2}, a pronounced non-linear increase in cell potential was observed, which coincides with the start of electro-oxidation of H_2S to S and the enhanced poisoning thereof. Moreover, Sethuraman et al. [17] propose an increase in the

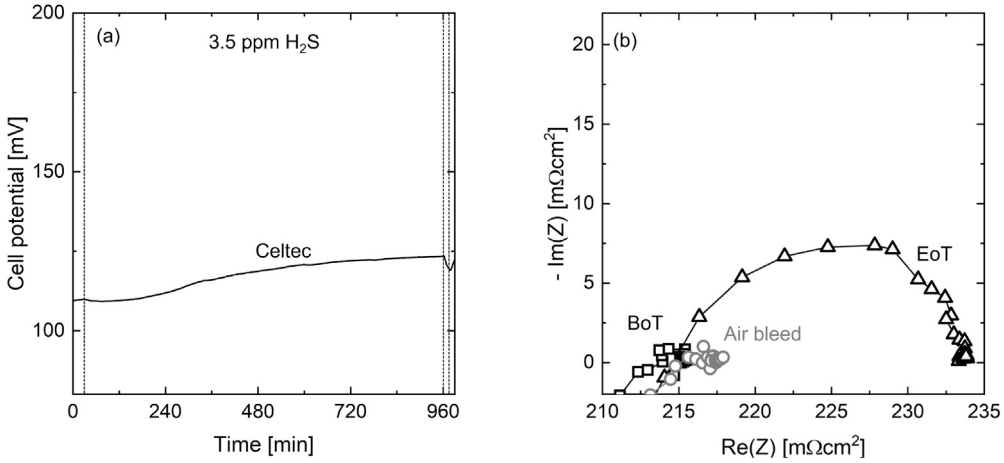

Fig. 8. (a) Cell potential over time a Celtec-EHC when adding 3.5 ppm H_2S to the EHC feed, no poison was introduced for the first 30 min and from 960 min to 975 min, vertical dashed lines indicate the change of gas composition, 500 mA cm^{-2}, $\lambda = 1.3$, 120 °C, 0.7 % RH; (b) Electrochemical impedance spectra of a Celtec MEA with 3.5 ppm H_2S BoT: squares, EoT: triangles, after air bleed: grey circles with 3.5 ppm H_2S.

adsorption degree of sulfur species until 500 mV vs. DHE and a decrease at higher potentials, which could also lead to more pronounced poisoning at elevated cell potentials. We hypothesize that the harmonic oscillations observed before the potential spike in our work are caused by the periodic adsorption and partial oxidation of sulfur species, which temporarily clean the catalyst surface and lower the cell potential.

Oscillating phenomena are reported for sulfide oxidation on Pt in an aqueous Na_2S solution [59]; however, they are not reported for the EHC or PEM fuel cells when H_2S is introduced. Jackson et al. [26] conducted the only EHC study investigating H_2S by operating a low-temperature EHC with reformate/H_2S mixtures under potentiostatic conditions. Upon the introduction of 100 ppb H_2S, the current decreased to 2 % of the current observed without poisoning. Due to the controlled potential in their study, the oxidation potential of sulfur species could not be reached, preventing the attainment of the second metastable state necessary for system oscillation. In contrast, our study examined H_2S poisoning in a high-temperature EHC under amperostatic conditions. As discussed earlier, Jackson et al. [27] and Mrusek et al. [10] report an exponential increase of cell potential in a low-temperature EHC when operating with 50 % H_2 in NG containing 0.78 % CO_2 and 1.8 ppm volatile sulfur compounds or 10 ppm THT, respectively. However, they did not observe oscillation in their low-temperature EHCs. As the mechanism why the oscillations occur is not yet clear, we can only hypothesize about the differences in our system. Both studies operate at significantly lower temperatures, leading to slower kinetics and lower catalyst availability [29]. The total poison concentration in both studies was higher, leading to more severe poisoning [35,57]. Additionally, the catalyst loading in our study was 2.3 times higher, and a different ionomer (H_3PO_4) was used.

Another reason for the increased poisoning could be the onset of CH_4 oxidation at 169 mV, and corresponding increased poisoning by the reaction products CO_2 and CO [26]. However, the oscillatory behavior was also observed when the feed gas was diluted with Ar instead of CH_4 (Fig. 9). Consequently, CH_4 oxidation does not significantly contribute to the observed behavior. When changing from CH_4 to Ar, the smaller oscillations leading to the self-oxidation are reduced (Fig. 9 (a), (b)). This minor change in oscillation pattern might be attributed to the additional poisoning of CO from CH_4 oxidation.

When increasing the relative humidity of the diluted feed to 6.5% (Fig. 9 (c)), the oscillation amplitude is increased, and there is no linear phase at low potentials before the exponential increase in cell potential, which could be caused by facilitated dissociative adsorption with more water present leading to enhanced poisoning. Moreover, catalyst recovery might be compromised by H_2S dissociation into HS^- upon desorption and HS^- being adsorbed again. The potential spike height is lowered to 0.9 V, and the frequency of the oscillation cycles is increased. This could be caused by faster sulfur oxidation when more water is present, as water is consumed in the sulfur oxidation (Eq. (19)) [60].

$$Pt{-}S + 2\,H_2O \longrightarrow SO_2 + 4\,H^+ + 4\,e^- + Pt \tag{19}$$

Similar to the observations from the Nafion-EHC with H_2S-poisoning, the potential continues to increase upon discontinuation of H_2S (Fig. 9 (c) from min. 240), which could be due to continuing dissociation of H_2S into HS^-. Additionally, H_2S previously adsorbed on the carbon support of the MEA might desorb and lead to continued poisoning of the catalyst. Due to the accelerating effect of water on H_2S poisoning of the EHC, the optimal humidification degree of the feed should be investigated.

The operation with CH_4-diluted H_2/H_2S becomes stabilized when operating the EHC at 160 °C (Fig. 7 (b), grey line). The cell potential increases by 10 mV upon adding H_2S to the feed, remains stable over 3.5 h, and drops by 7 mV when switching to pure H_2. The less severe effect of H_2S at 160 °C can be attributed to less adsorption of H_2S and a weakened Pt-S bond [61,62]. Additionally, the catalyst activity is increased, so less catalyst is needed to support the HOR.

In addition to the immediate effects of H_2S, a decline in the performance of the Celtec-MEA used for the H_2S poisoning experiments conducted was observed throughout the experiments and in the 16 h poisoning experiment. Consequently, the long-term effect of sulfur species on the EHC operation should be targeted in future investigations. The same Celtec-MEA was used for the H_2S experimental series. The performance decline is probably caused by the irreversible loss of catalytic activity when operating with H_2S, a phenomenon also reported for fuel cells. Hard-to-oxidize species are particularly formed at potentials above 500 mV, and the catalyst structure is altered. Consequently, exceeding this anode overpotential should be avoided in operation [17]. Detailed investigations on the poisoning mechanism of sulfur compounds would aid both developing operation strategies and catalyst development for sulfur poisoning management. In addition to the longer studies (>100 h) of the single poisons, poison mixtures, especially CO and H_2S, should be investigated for transferability to operation in natural gas.

3.5. *Poison mitigation strategies for* H_2S

The relative potential increase observed after 3.5 h poison operation with poison is summarized in Table 3. For all poisons, except H_2S

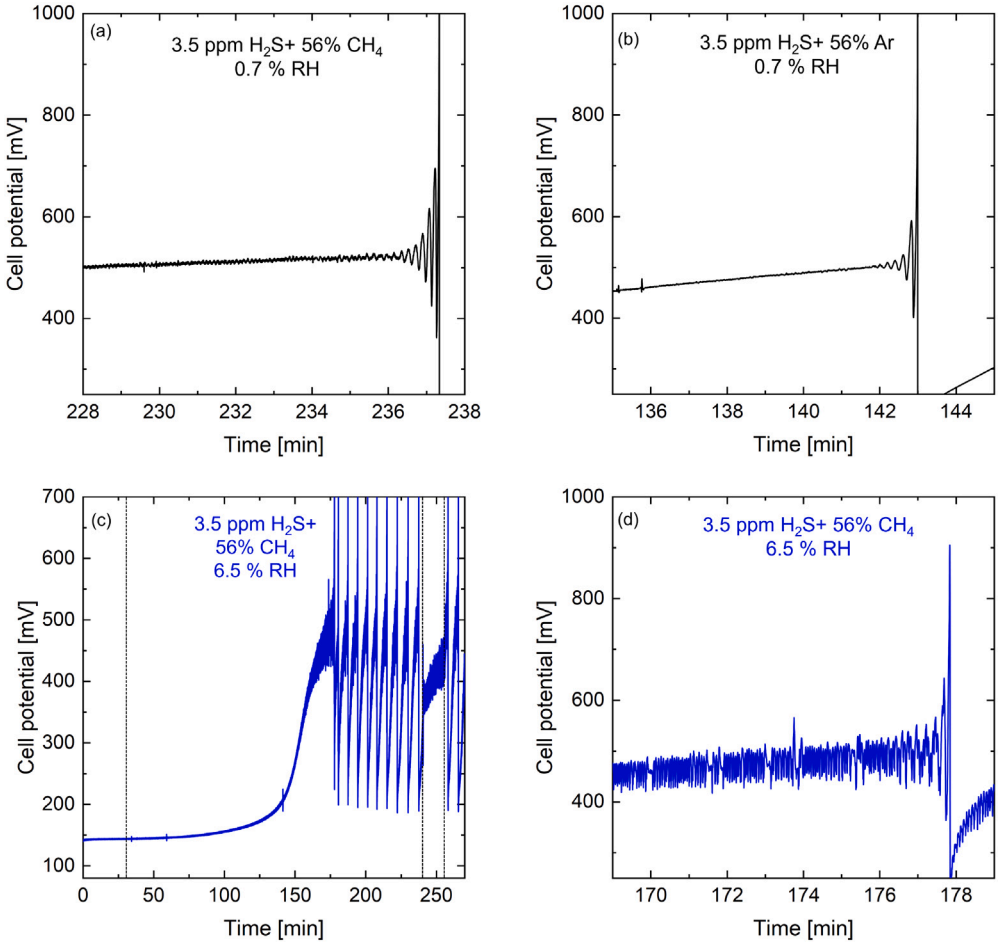

Fig. 9. Celtec-EHC at 500 mA cm^{-2} and 120 °C, with 3.5 ppm H_2S and 56 vol.% (a) Zoom in on oscillation with CH_4-diluted feed, with 3.5 ppm H_2S and 56 vol.% CH_4 with 0.7 % RH, (b) Zoom in on oscillation with Ar-diluted feed 56 vol.% Ar with 0.7 % RH (c) Cell potential over time of a Celtec-EHC at 500 mA cm^{-2} and 120 °C, with 3.5 ppm H_2S 56 vol.% CH_4 with 6.5 % RH, (d) Zoom in on oscillation with CH_4-diluted feed with 56 vol.% CH_4 and 6.5 % RH (blue).

Table 3
Summary of relative potential increase presented as mean value with standard deviation after operation with respective contaminant for 3.5 h at 500 mA cm^{-2}, Nafion-EHC: 70 °C, Celtec-EHC: 120 °C.

	Rel. potential increase [%]	
Contaminant	Nafion-EHC	Celtec-EHC
4 vol.% CO_2 in H_2	37.5 ± 5.5	4.7 ± 1.2
30 ppm CO in H_2	192 ± 28	5.7 ± 1.3
14 ppm NH_3 in H_2	3 ± 0.6	0.4 ± 0.4
3.5 ppm H_2S in H_2	192 ± 8.5	1.6 ± 0.2

with CH_4-dilutution, the potential increase for the Celtec-EHC during the poisoning experiments was lower than 6 %. Consequently, the investigation of poison mitigation strategies was focused on H_2S.

A 90 s air bleed at OCV was performed to mitigate the effect of operation with H_2S. During the air bleed, the O_2 from the air chemically oxidizes the adsorbed sulfur partially [63]. The EoT polarization performance of the Nafion-EHC remains 25 % increased compared to BoT, and ECSA was still reduced by 50 % after the air bleed (Fig. S3 (d) and S10 (b)). In comparison, Jackson et al. [26] could regain 40 % to 50 % of the current when operated without poison after 15 min offline O_2 treatment. After performing CV-cleaning, during which the adsorbed sulfur or H_2S is electrochemically oxidized (Eq. (19)), the BoT polarization performance and the ECSA of the Nafion-EHC could be restored (Fig. S3 (d) and S10 (b)). The potential cycles of the CV-cleaning of the Nafion-EHC are presented in Figure S11.

For the Celtec-EHC operated with H_2S in H_2 at 120 °C, the ECSA and the polarization behavior were not completely recovered after 90 s air bleed. In contrast, at 160 °C, the polarization behavior and ECSA was recovered by the air bleed (Fig. S4 (c) and S10 (b)). When operating the Celtec-EHC with CH_4-diluted H_2/H_2S, the ECSA and polarization behavior were recovered by five CV-cycles (Fig. S4 (e) and 10 (b)).

Increasing the operation temperature to 160 °C, as an online poison mitigation strategy, stabilizes the process and increases the voltage efficiency, which neglects heating, from 70 % to 90 %, but decreases the energy efficiency, which considers heating, from 49 % to 47 % (Fig. 10 (c)). Consequently, different poison mitigation strategies were analyzed regarding their effectiveness in stabilizing the process and process efficiency when operated with 3.5 ppm H_2S at 120 °C. Fig. 10 (a) presents the cell potential over time when air bleeds and CV-cleaning are employed as mitigation strategies. Applying periodic air bleeds for 5 min every 90 min at 120 °C avoided oscillations of the system, and the mean cell potential was reduced compared to the non-mitigated operation. Nonetheless, the cell potential at the end of the mitigation cycles increased over the cycles, indicating a non-reversible system recovery. This was also observed in the poisoning experiments, in which air bleeds at 120 °C could not wholly recover the ECSA at 120 °C or lower temperatures. Implementing air bleeds for the poisoning recovery necessitates additional equipment and downtime for flushing the cell to prevent oxyhydrogen formation. Additionally, introducing oxidants to the cell can enable H_2O_2 formation, leading to membrane degradation [34]. Moreover, studies on PEM water electrolysis revealed that shutdown periods, which are necessary to perform the air bleed,

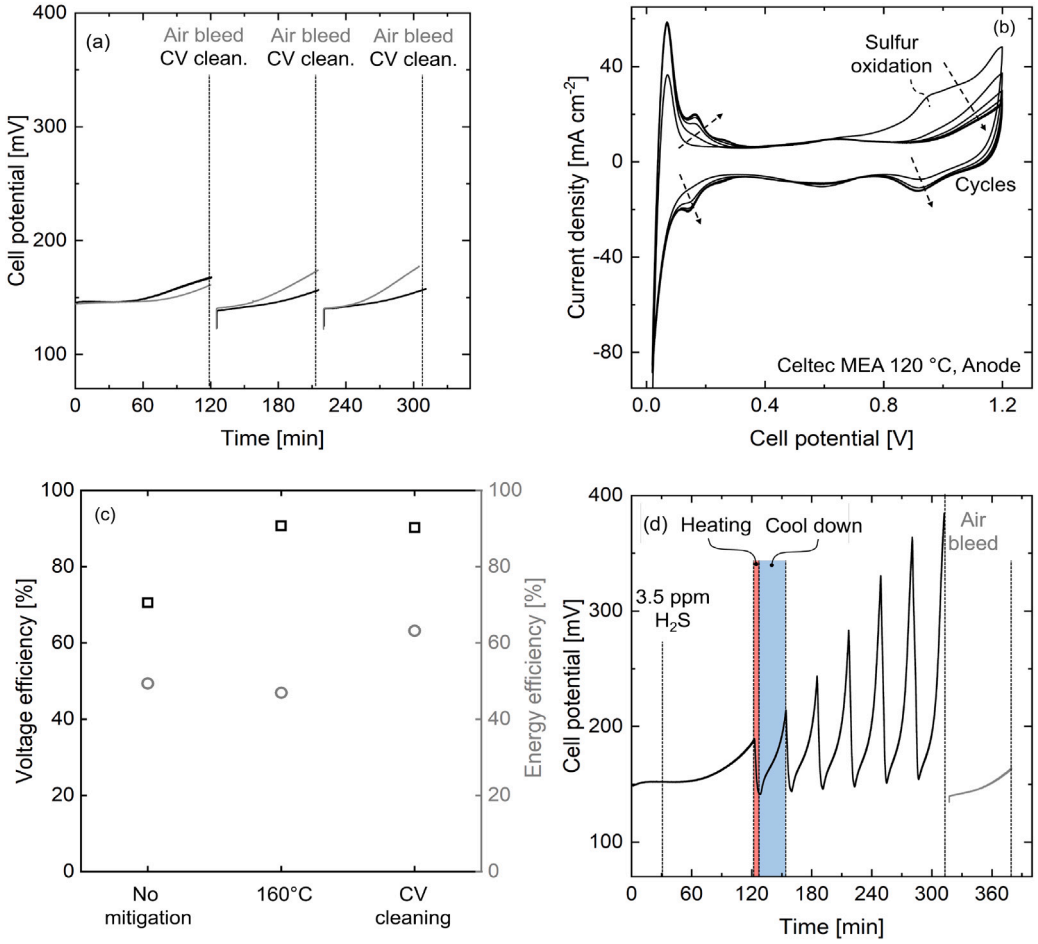

Fig. 10. (a) Poison mitigation of 3.5 ppm H_2S in 44 vol.% and 56 vol.% CH_4 by 5 min air bleeds and five cycles CV-cleaning of a Celtec-EHC at 120 °C, 0.7 % RH; (b) CV of Celtec-EHC after poisoning with 3.5 ppm H_2S in 44 vol.% H_2 and 56 vol.% CH_4, (c) Voltage and energy efficiency of the mitigated and unmitigated operation, calculated from the average cell potential, not considering the downtime during mitigation; (d) Poison mitigation of 3.5 ppm H_2S in 44 vol.% H_2 and 56 vol.% CH_4 by cyclic heating from 120 °C to 160 °C.

lead to a significant decrease in performance caused by increased HRF [64,65].

Periodic CV-cleaning every 90 min stabilizes the operation of the Celtec-EHC. Fig. 10 (b) shows the cyclic voltammogram of the CV-cleaning. The sulfur oxidation peak at potentials above 0.6 V decreases during the first three cycles until no significant changes can be observed in the CVs for cycles four and five. The reduction of oxidation charge and increase in PtO reduction charge in consecutive cycles indicate the removal of adsorbates. The energy efficiency and the voltage efficiency were improved by 14 % and 20 %, respectively, compared to the non-mitigated operation. However, Lopes et al. [63] observed catalyst degradation when performing CVs for H_2S poison mitigation. Additionally, Pt sulfides and oxides can be formed during CV cycling, which are difficult to remove [17]. Consequently, longer experiments operated with periodic CV cycles for poison mitigation should be performed to elucidate the possible degradation of the catalyst through the mitigation strategy. Moreover, the potential window of the cycles should be optimized to minimize the formation of sulfur oxides and catalyst degradation. Overall, applying offline mitigation strategies, such as air bleeds, leads to downtime for poison mitigation during operation, thereby reducing process efficiency. In this study, the downtime was neglected in the efficiency calculation. For CVs, no shutdown of the cell is necessary, although the H_2 production rate will vary. For a comprehensive evaluation, the mitigation strategies must be included in a techno-economic assessment to account for changes in MEA lifetime or energy efficiency they introduce to the system.

The cyclic heating protocol, shown in Fig. 10 (d), in which the cell was heated up to 160 °C periodically, although slowing the poisoning, did not yield a stable performance. Potentially, the operation time at 160 °C is too short to recover the poisoned catalyst surface sufficiently, and an exponential increase in cell potential is observed as the temperature drops back to 120 °C. Although this method could be optimized, applying it might cause accelerated component aging due to the mechanical stress imposed on the cell components by the temperature changes.

4. Conclusion

We provided a comprehensive characterization of low- (Nafion-EHC) and high-temperature EHC (Celtec-EHC) and elucidated the individual effect of CO_2, CO, NH_3, and H_2S on the EHC performance under galvanostatic operation. Strategies to reduce the adverse effects of H_2S on the Celtec-EHC were compared regarding efficiency and effectiveness. For the Nafion-EHC, operated at 70 °C, severe performance loss through poisoning was observed for CO_2, CO, and H_2S. The Celtec-EHC showed no significant performance decay when operated with CO_2 and CO at a moderate temperature of 120 °C. It was found that 14 ppm NH_3 will potentially lead to long-term performance degradation in both EHC types caused by ionomer alteration. The Celtec-EHC operation with 3.5 ppm H_2S in H_2 at 120 °C did not cause significant performance loss after 3.5 h, although a reduction in active catalyst area could be detected. However, when substituting 56 % of the H_2 in the mixture by

CH_4, the cell potential oscillated, and significant performance reduction was observed. When increasing the process temperature from 120 °C to 160 °C, the Celtec-EHC showed stable operation. However, the energy efficiency was impaired due to the increased need for heating power. Temperature pulsing and repeated air bleeds at 120 °C as mitigation strategies for the adverse effects of H_2S in diluted H_2 could not stabilize the performance. Repeated electro-oxidation using cyclic voltammetry results in a stable performance with reduced poisoning, although long-term catalyst degradation still needs to be evaluated.

This research elucidates the short-term effect of single contaminants in natural gas on EHC operation. This establishes a starting point for future studies, which must move beyond short-term single contaminant operation towards long-term stable treatment of real natural gas mixtures. The comparative study of Nafion and Celtec-EHC establishes a foundation for comprehensive techno-economic evaluations. Future work should target the long-term effects of NH_3 and H_2S on high-temperature EHCs and different mitigation strategies, especially at higher current densities. Additionally, hybrid processes, e.g., a combination of adsorption and EHC, for removing the most detrimental contaminants, such as H_2S and NH_3 before they enter the EHC, need to be assessed regarding economics.

CRediT authorship contribution statement

Wibke Zängler: Writing – review & editing, Writing – original draft, Visualization, Validation, Project administration, Methodology, Investigation, Formal analysis, Data curation, Conceptualization. **Nick Semrau:** Writing – review & editing, Visualization, Methodology, Investigation, Data curation, Conceptualization. **Matthias Wessling:** Writing – review & editing, Supervision, Resources, Project administration, Funding acquisition. **Robert Keller:** Writing – review & editing, Supervision, Resources, Project administration, Funding acquisition, Formal analysis, Conceptualization.

Declaration of Generative AI and AI-assisted technologies in the writing process

During the preparation of this work the author(s) used Grammarly in order to revise spelling and grammar. After using this tool/service, the author(s) reviewed and edited the content as needed and take(s) full responsibility for the content of the publication.

Declaration of competing interest

The authors declare that they have no known competing financial interests or personal relationships that could have appeared to influence the work reported in this paper.

Acknowledgments

This work was funded by the German Federal Ministry for Education and Research (BMBF) within the project HyInnoSep of Zukunftcluster Wasserstoff [grant number 03ZU1115CA]. M. Wessling acknowledges DFG funding through the Gottfried Wilhelm Leibniz Award 2019 [WE 4678/12-1]. This work was conducted in part at the Competence Center Industrial Electrochemistry ELECTRA, which is supported by the "European Regional Development Fund" (ERDF) and the Federal State of North Rhine-Westphalia [grant number ERDF 0500077]. The authors thank Alexander Jachertz, Sandra Gelbach, and Karin Faensen for their support.

Appendix A. Supplementary data

Supplementary material related to this article can be found online at https://doi.org/10.1016/j.ijhydene.2025.150980.

References

[1] Pawelec G, Muron M, Bracht J, Bonnet-Cantalloube B, Floristean A, Brahy N. Hydrogen demand and supply in the EU. Tech. rep., Hydrogen Europe Intelligence Department; 2020, Hydrogen Europe Clean Hydrogen Monitor. https://hydrogeneurope.eu/hydrogen-transport-distribution.

[2] Kanellopoulos K, Busch S, De Felice M, Giaccaria S, Costescu A. Blending hydrogen from electrolysis into the European gas grid a joint modelling assessment of the European power and gas systems with METIS. Tech. rep. EUR 30951 EN, Publications Office of the European Union; 2022, http://dx.doi.org/10.2760/908387.

[3] Mahajan D, Tan K, Venkatesh T, Kileti P, Clayton CR. Hydrogen Blending in Gas Pipeline Networks—A Review. Energies 2022;15(10):3582. http://dx.doi.org/10.3390/en15103582.

[4] Relvas F, Whitley RD, Silva C, Mendes A. Single-Stage Pressure Swing Adsorption for Producing Fuel Cell Grade Hydrogen. Ind Eng Chem Res 2018;57(14):5106–18. http://dx.doi.org/10.1021/acs.iecr.7b05410.

[5] Nordio M, Wassie SA, Van Sint Annaland M, Pacheco Tanaka DA, Viviente Sole JL, Gallucci F. Techno-economic evaluation on a hybrid technology for low hydrogen concentration separation and purification from natural gas grid. Int J Hydrog Energ 2021;46:23417–35. http://dx.doi.org/10.1016/j.ijhydene.2020.05.009.

[6] Melaina M, Antonia O, Penev M. Blending hydrogen into natural gas pipelines networks: a review of key issues. Tech. rep., Golden, Colorado: National Renewable Energy Laboratory; 2013, NREL/TP-500-51995.

[7] Langer SH, Hademan RG. Electrolytic hydrogen purification and recovery of same. 1969, US 3475302.

[8] Maget HJR. Process for Gas Purification. 1970, US 3489670.

[9] Nordio M, Rizzi F, Manzolini G, Mulder M, Raymakers L, Van Sint Annaland M, et al. Experimental and modelling study of an electrochemical hydrogen compressor. Chem Eng J 2019;369:432–42. http://dx.doi.org/10.1016/j.cej.2019.03.106.

[10] Mrusek S, Blasius M, Morgenroth F, Thiele S, Wasserscheid P. Hydrogen extraction from methane-hydrogen mixtures from the natural gas grid by means of electrochemical hydrogen separation and compression. Int J Hydrog Energ 2024;50(Part A):526–38. http://dx.doi.org/10.1016/j.ijhydene.2023.08.195.

[11] Durmus GNB, Colpan CO, Devrim Y. A review on the development of the electrochemical hydrogen compressors. J Power Sources 2021;494:229743. http://dx.doi.org/10.1016/j.jpowsour.2021.229743.

[12] Zou J, Han N, Yan J, Feng Q, Wang Y, Zhao Z, et al. Electrochemical Compression Technologies for High-Pressure Hydrogen: Current Status, Challenges and Perspective, electrochem. Energy Rev 2020;3(4):690–729. http://dx.doi.org/10.1007/s41918-020-00077-0.

[13] Trégaro M, Rhandi M, Druart F, Deseure J, Chatenet M. Electrochemical hydrogen compression and purification versus competing technologies: Part II. Challenges in electrocatalysis. Chin J Catal 2020;41(5):770–82. http://dx.doi.org/10.1016/S1872-2067(19)63438-8.

[14] DVGW German Technical and Scientific Association for Gas and Water, DVGW G 260 (A) - Gasbeschaffenheit. 2021.

[15] Valdés-López VF, Mason T, Shearing PR, Brett DJ. Carbon monoxide poisoning and mitigation strategies for polymer electrolyte membrane fuel cells – a review. Prog Energy Combust Sci 2020;79:100842. http://dx.doi.org/10.1016/j.pecs.2020.100842.

[16] Nordio M, Eguaras Barain M, Raymakers L, Van Sint Annaland M, Mulder M, Gallucci F. Effect of CO_2 on the performance of an electrochemical hydrogen compressor. Chem Eng J 2020;392:123647. http://dx.doi.org/10.1016/j.cej.2019.123647.

[17] Sethuraman VA, Weidner JW. Analysis of sulfur poisoning on a PEM fuel cell electrode. Electrochim Acta 2010;55(20):5683–94. http://dx.doi.org/10.1016/j.electacta.2010.05.004.

[18] Dong W, Xu C, Zhao W, Xin M, Xiang Y, Zheng A, et al. Poisoning Effects of H_2S, C_2S, and COS on Hydrogen Oxidation Reaction over Pt/C Catalysts. ACS Appl Energy Mater 2022;5(10):12640–50. http://dx.doi.org/10.1021/acsaem.2c02284.

[19] Farooque M, Fahidy TZ. Low Potential Oxidation of Hydrogen Sulfide on a Rotating Tripolar Wiper-Blade Electrode via Continuous Anode Reactivation. J Electrochem Soc 1977;124(8):1191–5. http://dx.doi.org/10.1149/1.2133526.

[20] Gomez YA, Oyarce A, Lindbergh G, Lagergren C. Ammonia Contamination of a Proton Exchange Membrane Fuel Cell. J Electrochem Soc 2018;165(3):F189. http://dx.doi.org/10.1149/2.0761803.

[21] Vermaak L, Neomagus HW, Bessarabov DG. Recent advances in membrane-based electrochemical hydrogen separation: A review. Membranes 2021;11(2):127. http://dx.doi.org/10.3390/membranes11020127.

[22] Halseid R, Vie PJ, Tunold R. Effect of ammonia on the performance of polymer electrolyte membrane fuel cells. J Power Sources 2006;154:343–50. http://dx.doi.org/10.1016/j.jpowsour.2005.10.011.

[23] Isorna Llerena F, de las Heras Jiménez A, López González E, Segura Manzano F, Andújar Márquez JM. Effects of Ammonia Impurities on the Hydrogen Flow in High and Low Temperature Polymer Electrolyte Fuel Cells. Fuel Cells 2019;19(6):651–62. http://dx.doi.org/10.1002/fuce.201900031.

[24] Schonvogel D, Büsselmann J, Schmies H, Langnickel H, Wagner P, Dyck A. High temperature polymer electrolyte membrane fuel cell degradation provoked by ammonia as ambient air contaminant. J Power Sources 2021;502:229993. http://dx.doi.org/10.1016/j.jpowsour.2021.229993.
[25] Uribe FA, Gottesfeld S, Zawodzinski TA. Effect of Ammonia as Potential Fuel Impurity on Proton Exchange Membrane Fuel Cell Performance. J Electrochem Soc 2002;149(3):A293–6. http://dx.doi.org/10.1149/1.1447221.
[26] Jackson C, Raymakers LF, Mulder MJ, Kucernak AR. Poison mitigation strategies for the use of impure hydrogen in electrochemical hydrogen pumps and fuel cells. J Power Sources 2020;472:228476. http://dx.doi.org/10.1016/j.jpowsour.2020.228476.
[27] Jackson C, Smith G, Kucernak AR. Deblending and purification of hydrogen from natural gas mixtures using the electrochemical hydrogen pump. Int J Hydrog Energ 2023;52(Part B):816–26. http://dx.doi.org/10.1016/j.ijhydene.2023.05.065.
[28] International Organization for Standardization. ISO/DIS 14687:2024 Hydrogen fuel quality - Product specification. 2024.
[29] Perry KA, Eisman GA, Benicewicz BC. Electrochemical hydrogen pumping using a high-temperature polybenzimidazole (PBI) membrane. J Power Sources 2008;177(2):478–84. http://dx.doi.org/10.1016/j.jpowsour.2007.11.059.
[30] Lim KH, Matanovic I, Maurya S, Kim Y, De Castro ES, Jang JH, et al. High Temperature Polymer Electrolyte Membrane Fuel Cells with High Phosphoric Acid Retention. ACS Energy Lett 2023;8(1):529–36. http://dx.doi.org/10.1021/acsenergylett.2c02367.
[31] Vermaak L, Neomagus HWJP, Bessarabov DG. Hydrogen Separation and Purification from Various Gas Mixtures by Means of Electrochemical Membrane Technology in the Temperature Range 100–160°C. Membranes 2021;11(4):282. http://dx.doi.org/10.3390/membranes11040282.
[32] Maxwell DS, Sun Q, Rojas H, Kendrick R, Pavlicek RK, Castro ESD, et al. High Purity Hydrogen Separation with HT-PBI Based Electrochemical Pump Operation at 120°C. J Electrochem Soc 2023;170:034510. http://dx.doi.org/10.1149/1945-7111/acc6f7.
[33] Arunagiri K, Turssline JM, Arges CG. Purifying Hydrogen from Dilute Hydrogen - Natural Gas Mixtures Using HT-PEM Electrochemical Hydrogen Pumps. ACS Energy Lett 2024;9(6):2912–29. http://dx.doi.org/10.1021/acsenergylett.4c00746.
[34] Rui Z, Hua K, Dou Z, Tan A, Zhang C, Shi X, et al. A new insight into the chemical degradation of proton exchange membranes in water electrolyzers. J Mat. Chem A 2024;12(16):9563–73.
[35] Durmus GNB, Colpan CO, Devrim Y. Investigation of the performance of high-temperature electrochemical hydrogen purification from reformate gases. Int J Energy Res 2022;46(8):11443–55. http://dx.doi.org/10.1002/er.7940.
[36] Chhetri M, Leonard DP, Maurya S, Sharan P, Kim Y, Kozhushner A, et al. Electrochemical pumps based on ion-pair membranes for separation of hydrogen from low-concentration mixtures. Nat Energy 2024;9:1517–28. http://dx.doi.org/10.1038/s41560-024-01669-6.
[37] Lukaszewski M, Soszko M, Czerwiński A. Electrochemical methods of real surface area determination of noble metal electrodes - an overview. Int J Electrochem Sci 2016;11(6):4442–69. http://dx.doi.org/10.20964/2016.06.71.
[38] Trasatti S, Petrii O. Real surface area measurements in electrochemistry. J Electroanal Chem 1992;327(1–2):353–76. http://dx.doi.org/10.1016/0926-860x(96)80148-7.
[39] Zhang JZ, Liu Z, Goodwin JG. The effect of low concentrations of CO on H_2 adsorption and activation on Pt/C. Part 1: In the absence of humidity. J Power Sources 2010;195(10):3060–8. http://dx.doi.org/10.1016/j.jpowsour.2009.11.124.
[40] Ke S, Cui B, Sun C, Qin Y, Zhang J, Dou M. Intriguing H_2s Tolerance of the PtRu Alloy for Hydrogen Oxidation Catalysis in PEMFCs: Weakened Pt–s Binding with Slower Adsorption Kinetics. ACS Appl Mater Interfaces 2022;14(42):47765–74. http://dx.doi.org/10.1021/acsami.2c13742.
[41] Hayes M, Kuhn A. Determination of platinum catalyst surface area with potentiodynamic techniques — Effect of experimental parameters. Appl Surf Sci 1980;6(1):1–14. http://dx.doi.org/10.1016/0378-5963(80)90050-1.
[42] Grigoriev SA, Shtatniy IG, Millet P, Porembsky VI, Fateev VN. Description and characterization of an electrochemical hydrogen compressor/concentrator based on solid polymer electrolyte technology. Int J Hydrog Energ 2011;36(6):4148–55. http://dx.doi.org/10.1016/j.ijhydene.2010.07.012.
[43] Borisov G, Borisov N, Heiss J, Schnakenberg U, Slavcheva E. PEM Electrochemical Hydrogen Compression with Sputtered Pt Catalysts. Membranes 2023;13(6):594. http://dx.doi.org/10.3390/membranes13060594.
[44] Ma Y-L, Wainright JS, Litt MH, Savinell RF. Conductivity of PBI Membranes for High-Temperature Polymer Electrolyte Fuel Cells. J Electrochem Soc 2004;151(1):A8–16. http://dx.doi.org/10.1149/1.1630037.
[45] Pineda-Delgado JL, Chávez-Ramirez AU, C. K. Gutierrez B, Rivas S, Marisela CR, de Jesús Hernández-Cortes R, et al. Effect of relative humidity and temperature on the performance of an electrochemical hydrogen compressor. Appl Energy 2022;311:118617. http://dx.doi.org/10.1016/j.apenergy.2022.118617.
[46] Sdanghi G, Dillet J, Didierjean S, Fierro V, Maranzana G. Feasibility of Hydrogen Compression in an Electrochemical System: Focus on Water Transport Mechanisms. Fuel Cells 2020;20(3):370–80. http://dx.doi.org/10.1002/fuce.201900068.
[47] Melchior JP, Majer G, Kreuer KD. Why do proton conducting polybenzimidazole phosphoric acid membranes perform well in high-temperature PEM fuel cells? Phys Chem Chem Phys 2017;19(1):601–12. http://dx.doi.org/10.1039/c6cp05331a.
[48] Schalenbach M, Hoefner T, Paciok P, Carmo M, Lueke W, Stolten D. Gas Permeation through Nafion. Part 1: Measurements. J Phys Chem C 2015;119(45):25145–55. http://dx.doi.org/10.1021/acs.jpcc.5b04155.
[49] Chen Y, Azizi K, Zhang W, Aili D, Primdahl S, Cleemann LN, et al. Feasibility of using thin polybenzimidazole electrolytes in high-temperature proton exchange membrane fuel cells. Int J Hydrog Energ 2022;47(66):28615–25. http://dx.doi.org/10.1016/j.ijhydene.2022.06.156.
[50] He R, Li Q, Bach A, Jensen JO, Bjerrum NJ. Physicochemical properties of phosphoric acid doped polybenzimidazole membranes for fuel cells. J Membr Sci 2006;277(1–2):38–45. http://dx.doi.org/10.1016/j.memsci.2005.10.005.
[51] McPherson IJ, Ash PA, Jones L, Varambhia A, Jacobs RM, Vincent KA. Electrochemical CO Oxidation at Platinum on Carbon Studied through Analysis of Anomalous in Situ IR Spectra. J Phys Chem C 2017;121(32):17176–87. http://dx.doi.org/10.1021/acs.jpcc.7b02166.
[52] Gardner CL, Ternan M. Electrochemical separation of hydrogen from reformate using PEM fuel cell technology. J Power Sources 2007;171(2):835–41. http://dx.doi.org/10.1016/j.jpowsour.2007.06.020.
[53] Jusys Z, Behm RJ. Electrooxidation of CO and H_2/CO mixtures on a carbon-supported Pt catalyst—a kinetic and mechanistic study by differential electrochemical mass spectrometry. Phys Chem Chem Phys 2001;3(21):4650–60. http://dx.doi.org/10.1021/jp011510y.
[54] Halseid R, Wainright JS, Savinell RF, Tunold R. Oxidation of Ammonium on Platinum in Acidic Solutions. J Electrochem Soc 2007;154(2):B263. http://dx.doi.org/10.1149/1.2405851.
[55] Soto HJ, Lee WK, Van Zee JW, Murthy M. Effect of transient ammonia concentrations on PEMFC performance. Electrochem Solid-State Lett 2003;6(7):A133–5. http://dx.doi.org/10.1149/1.1574651.
[56] Huang F, Pingitore AT, Benicewicz BC. High Polymer Content m/p-Polybenzimidazole Copolymer Membranes for Electrochemical Hydrogen Separation under Differential Pressures. J Electroch. Soc 2020;167(6):063504. http://dx.doi.org/10.1149/1945-7111/ab81a0.
[57] Shi W, Yi B, Hou M, Shao Z. The effect of H2S and CO mixtures on PEMFC performance. Int J Hydrog Energ 2007;32(17):4412–7. http://dx.doi.org/10.1016/j.ijhydene.2007.06.029.
[58] Zolfaghari A, Chayer M, Jerkiewicz G. Energetics of the Underpotential Deposition of Hydrogen on Platinum Electrodes: I. Absence of Coadsorbed Species. J Electrochem Soc 1999;146(11):4158. http://dx.doi.org/10.1149/1.1837955.
[59] Feng J, Gao Q, Xu L, Wang J. Nonlinear phenomena in the electrochemical oxidation of sulfide. Electrochem Commun 2005;7(12):1471–6. http://dx.doi.org/10.1016/j.elecom.2005.10.004.
[60] Loucka T. Adsorption and oxidation of sulphur and of sulphur dioxide at the platinum electrode. J Electroanal Chem 1971;31(2):319–32. http://dx.doi.org/10.1016/S0022-0728(71)80162-6.
[61] Ke S, Sun C, Cui B, Qin Y, Dou M. Operatable and Efficient Mitigation Strategies for H2S Poisoning in Proton Exchange Membrane Fuel Cells: Releasing Pt Reactive Sites for Hydrogen Oxidation. ACS Appl Energy Mater 2023;6(6):3337–46. http://dx.doi.org/10.1021/acsaem.2c04026.
[62] Mohtadi R, Lee WK, Van Zee JW. The effect of temperature on the adsorption rate of hydrogen sulfide on Pt anodes in a PEMFC. Appl Catal B: Environmetal 2005;56(1–2):37–42. http://dx.doi.org/10.1016/j.apcatb.2004.08.012.
[63] Lopes T, Paganin VA, Gonzalez ER. Hydrogen sulfide tolerance of palladium-copper catalysts for PEM fuel cell anode applications. Int J Hydrog Energ 2011;36(21):13703–7. http://dx.doi.org/10.1016/j.ijhydene.2011.07.126.
[64] Kuhnert E, Mayer K, Heidinger M, Rienessel C, Hacker V, Bodner M. Impact of intermittent operation on photovoltaic-PEM electrolyzer systems: A degradation study based on accelerated stress testing. Int J Hydrog Energ 2024;55:683–95. http://dx.doi.org/10.1016/j.ijhydene.2023.11.249.
[65] Weiß A, Siebel A, Bernt M, Shen T-H, Tileli V, Gasteiger HA. Impact of Intermittent Operation on Lifetime and Performance of a PEM Water Electrolyzer. J Electrochem Soc 2019;166(8):F487–97. http://dx.doi.org/10.1149/2.0421908jes.